PentaFluoroStyrene-based block copolymers controlled self-assembly pattern: A platform paving the way to functional block copolymers

Karell Bosson, Pierre Marcasuzaa, Antoine Bousquet, Günter E.M. Tovar, Vladimir Atanasov, Laurent Billon

PentaFluoroStyrene-based Block Copolymers Controlled Self-Assembly Pattern: a platform paving the way to functional block copolymers

Karell Bosson,[1,2,3] Pierre Marcasuzaa,[1,2] Antoine Bousquet,[2] Günter E.M. Tovar,[4,5] Vladimir Atanasov,[3] Laurent Billon[1, 2]

[1] Bio-inspired Materials Group: Functionalities & Self-assembly, E2S UPPA, 64000 Pau, France

[2] Universite de Pau et Pays de l'Adour, E2S UPPA, CNRS, IPREM, UMR5254, 64000 Pau, France

[3] Institute of Chemical Process Engineering, University of Stuttgart, Stuttgart, Germany

[4] Institute for Interfacial Process Engineering and Plasma Technology IGVP, University of Stuttgart, Pfaffenwaldring 31, 70569 Stuttgart, Germany

[5] Fraunhofer Institute for Interfacial Engineering and Biotechnology IGB, Nobelstr. 12, 70569 Stuttgart, Germany

Corresponding author: laurent.billon@univ-pau.fr

Highlights

- Diblock copolymers of 2,3,4,5,6-pentafluorostyrene (PFS) and butyl acrylate (BuA) synthesized by nitroxide mediated polymerization (NMP) with a large range of molar compositions and molecular weights.
- Nano-phase separation in thin films due to the high immiscibility of both polymeric blocks.
- Versatile self-assembly from *out-of-the-plane* PPFS to PBuA cylinders crossing through lamellar morphology.
- Functionalization of the PPFS block by *para* fluorine-thiol soft organo-catalysed substitution.
- Screening the nano-phase separation by matching the solubility parameters of the modified PFS and BuA monomer units.

Graphical abstract

Abstract

Diblock copolymers of 2,3,4,5,6-pentafluorostyrene (PFS) and butyl acrylate (BuA) were synthesized by nitroxide mediated polymerization (NMP). By varying the conversion and/or the BuA monomer to PPFS macro-initiator ratio, various molar compositions of the block copolymer BCP were obtained. Due to the immiscibility of both polymeric blocks, phase separation at the nanometre scale occurred. The variety of BCP synthesized gave rise to a large panel of morphologies by self-assembly. The structuration of the nanodomains of PPFS/PBuA BCPs were studied by AFM and SAXS. Nanodomain sizes ranging from 30 to 45 nm depending on the molar mass of the BCP were observed. Moreover, the lability of the fluorine atom in *para* position of the aromatic ring of the PFS units allows for the functionalization of the BCPs. Indeed, the *para* fluorine-thiol soft organo-catalysed substitution was performed with 1-hexanethiol as side group. The thermal properties and the self-assembly pattern of the BCP changes drastically by the incorporation of alkyl moiety, acting as an artificial increase of the volume fraction of the PPFS block and also matching the solubility parameter value of the PBA block, *i.e.* no more nano-pattern is observed by AFM and SAXS.

Keywords: nitroxide-mediated polymerization, poly(pentafluorostyrene), Block copolymers, self-assembly, *para* fluorine-thiol modification

1. Introduction

Fluorinated polymers are well known for their thermal, chemical, and physical stability. For that reason, they can be used for sensors and cable insulation, membranes, packaging, sealing materials or chemical resistant components. [1] Among them, the most famous polymers are poly(vinylidene fluoride) (PVDF), poly(tetrafluoroethylene) (PTFE), or poly(vinyl fluoride) (PVF). Moreover, fluorinated polymers belong to the category of low surface energy materials, due to their relatively low attraction to other molecules. Therefore, their interfacial energy is low, leading to easy segregation. [2] All those properties make them suitable candidates over the synthesis for the self-assembly of block copolymers (BCPs). BCPs have gained interest throughout the years for the development of materials with novel properties. Indeed, BCPs with immiscible blocks, can microphase separate to form ordered structures. The parameters dictating the phase separation are the volume fraction Φ of both blocks in the BCP and the χN segregation product, where χ is the Flory-Huggins parameter (χAB) which represents the degree of incompatibility between both blocks and N represents the total degree of polymerization. Depending on the combination of both parameters, different morphologies can be targeted from the self-assembly of BCPs. [3] Properties of such final materials are a combination of the intrinsic properties of the individual polymers forming the blocks at the nanometer scale as well as at the macrometer scale. Thus, there is an interest in having custom-made BCPs for diverse applications such as: drug delivery and release, [4,5] biomaterials, [6] lithography for data storage, [7] or thermoplastic materials. [8]

Multiple techniques exist to synthesize BCPs, one of them is multi step living polymerization such as ionic (IP) or controlled radical polymerizations (CRP). [3] These polymerization techniques allow for the synthesis of polymers with controlled degree of polymerization and narrow dispersity. Compared to the living ionic polymerization, CRP does not require strict synthetic conditions and a wide variety of functional monomers can be

polymerized, which makes it an easier method for the design of BCPs. Within CRP, different techniques were developed for almost a quarter of century. [9,10,11] The most used are: nitroxide-mediated polymerization (NMP) [12], atom transfer radical polymerization (ATRP) [13] and reversible addition-fragmentation chain transfer (RAFT) [14] radical polymerization. They are differentiated by the reversible termination reaction controlling of the chain growth. The NMP technique, uses an alkoxyamine compound that divides into a radical (initiator) and a nitroxide counter-radical (controlling agent) upon heat. It can react reversibly with the propagating species to put them in a dormant state, creating a macro-initiator that can be used to initiate the polymerization of another monomer to make BCPs. In ATRP, the initiator carries a transferable halogen, and a transition metal catalyst and some additives are needed to carry out the reaction. The technique uses a reversible redox process catalysed by the metal/ligand catalyst complex. There is a need for the removal of the catalyst after reaction. Finally, the RAFT process uses a transfer agent that is specific to the type of monomer to perform the reversibility of the mechanism, in addition to a classic radical initiator. NMP was the chosen technique for the experiments as it is easy to implement with only one compound that gives both an initiator and a controlling agent. Furthermore, there is no need of the removal of the reagent after the reaction and the alkoxyamine could be used for a variety of monomers.

We report here on the efficient synthesis of poly(pentafluorostyrene)-*block*-poly(butyl acrylate) PPFS-*b*-PBuA block copolymers (**Scheme 1**).

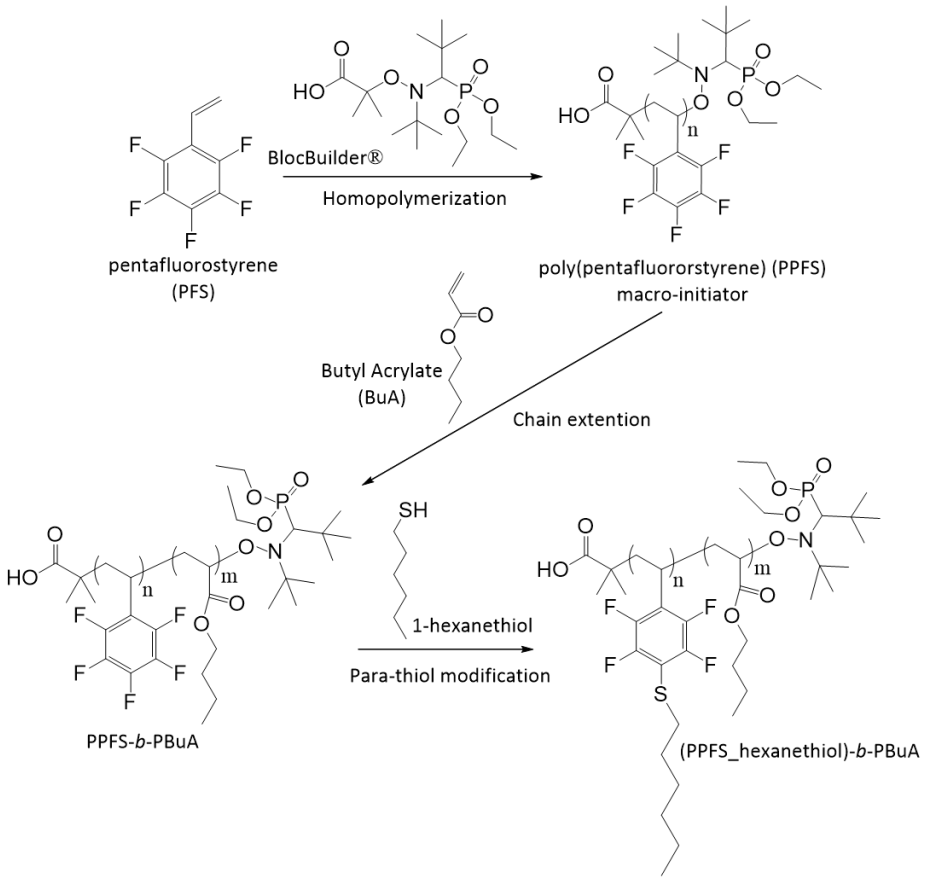

Scheme 1. Synthetic route of the PPFS-*b*-PBuA block copolymers and their 1-hexanethiol modified homologues.

We firstly discuss the synthesis of PPFS/PBuA by NMP using the BlocBuilder® initiator as an efficient controlled radical polymerization. Controlled radical polymerization of BCPs using poly(pentafluorostyrene) have already been reported in the literature, but mainly by ATRP. [15,16,17,18,19,20] Few examples can also be found describing NMP [21,22,23] or RAFT [24] polymerizations methods. Additionally, PPFS can be easily modified due to the accessibility of the fluorine in *para*-position of the phenylene group, allowing for countless possibilities for polymer functionalization by nucleophilic substitution. Over the year's attractive post-modification techniques such as click-chemistry have been used for the ease they provide to functionalize polymers. Click-chemistry for *para* fluorine substitutions with azide [25] and thiol [26,27,28] have already been proposed for PPFS. In the second part of this

manuscript, the successful *para* fluoro-thiol modification of the BCPs was performed with 1-hexanethiol (HT) to explore the impact of the alkyl chain on both the glass temperature transition *Tg* and the self-assembly properties of the derivatives BCP. Indeed, the *para*-addition of 1-hexanethiol gives some mobility to the polymer chains. Thus, a brittle to flexible transition is determined by DSC and macroscopically. Additionally, the self-assembly of the BCPs before and after modification with 1-hexanethiol was studied by AFM and SAXS.

2. Experimental section

2.1. Materials

Pentafluorostyrene (99%, Sigma-Aldrich), butyl acrylate (99%, Sigma-Aldrich), BlocBuilder® (Provided by Arkema), free-SG1 (83%, Provided by Arkema), dimethylformamide (DMF, anhydrous, 99.8%, Sigma-Aldrich), 1-hexanethiol (95%, Sigma-Aldrich), 1,8-Diazabicyclo[5.4.0]undec-7-ene (DBU, 99%, Sigma, Aldrich), technical methanol (VWR), and THF (VWR), were used without further purification.

2.2. PPFS homopolymers and their Block copolymers homologues

2.2.1. Homopolymerization of PFS.

The NMP of PFS was performed in bulk following a typical NMP procedure. Pentafluorostyrene (41.2 mmol), BlocBuilder® (0.10 mmol) and some free-SG1 (0.01 mmol) were added to a 25mL round bottom flask equipped with rubber seals and a magnetic stirring bar. The mixture was placed into an ice bath and bubbled with nitrogen for 15 minutes and subsequently placed into an oil bath that was pre-heated at 115°C. The mixture was left to stir for 5h at 115°C. The polymer was recovered by precipitation of the reaction mixture into methanol, after cooling down to room temperature. The precipitation was followed by filtration and drying of the polymer under vacuum oven at 60°C overnight. Purification of the polymer

was performed by dissolution in THF and subsequent precipitation in methanol. The purification step was repeated twice, PPFS was obtained (conversion: 60%).

2.2.2. Chain extension of PPFS with BuA to yield PPFS-b-PBuA

The previously synthesized PPFS were used as a macro-initiator for the chain extension procedure with butyl acrylate (BuA) monomer. To do so, in a 25mL round bottom flask was equipped with rubber seals and a magnetic stirring bar, the macro-NMP PPFS initiator (0.078 mmol) and some free-SG1 (0.0078 mmol) were dissolved into DMF (1.5 mL). Followed by the addition of BuA (35.7 mmol) in the mixture. Different ([BuA]/[PPFS]) ratios were calculated and used to target different self-assembly morphologies. The mixture was degassed with nitrogen at room temperature for 15 minutes before putting the flask in an oil bath pre-heated at 115°C. The mixture was left to stir at 115°C for 9h. For the other BCP compositions, the monomers ratios and time of reaction were varied depending on the targeted monomer conversion. The BCP was recovered by precipitation of the mixture into methanol, after cooling down to room temperature. The precipitation was followed by filtration and drying of the polymer under vacuum oven at 60°C overnight (conversion: 28%).

2.2.3. Para-thiol modification of the diblock copolymers

In an adequate round bottom flask, the block copolymer BCP3 (0.44 g, 0.74 mmol, 1 *eq*) was dissolved into DMF (5 mL). DBU (0.117 g, 0.78 mmol, 1.05 *eq*) was added to the mixture followed by the addition of 1-hexanethiol (0.092 g, 0.82 mmol, 1.1 *eq*). The mixture was left to stir at room temperature overnight to reach full modification. The reacted solution was precipitated into methanol twice to remove residual chemicals and dried under vacuum at 30°C overnight.

3. Characterization Methods

3.1. ^{1}H NMR, DOSY NMR & ^{19}F NMR

NMR spectra were recorded on a Bruker DPX-400 spectrometer using deuterated solvents obtained from Sigma-Aldrich ($CDCl_3$). The spectra were recorded at room temperature.

3.2. Size Exclusion Chromatography (SEC)

The molar mass of the polymers was determined by Size Exclusion Chromatography. The materials were dissolved in THF at a concentration of 3 g/L, Toluene was used as a flow marker. Prior to injection, the samples were filtered through 0.45 µm nylon filter. The analysis was performed at 30°C at a flow rate of 1ml/min. The set up consisted of a pump (LC-20A, Shimadzu), an autosampler (Sil- 20AHT), a differential refractometer (Optilab Rex, Wyatt), and three columns in series (Styragel HR2, HR4 and HR6 with pore sizes ranging from 102 to 106 Å).

3.3. Differential Scanning Calorimetry (DSC)

Between 1 to 10 mg of polymer was placed into aluminium capsules that were closed hermetically. The capsule was then placed into the DSC device (DSC Q100 from TA instruments) that was set to heating and cooling rates of 20°C/min under nitrogen atmosphere at a flow of 50 mL/min. The characterization was performed at the temperature range of -80°C to 180°C.

3.4. Atomic force microscopy (AFM) & self-assembly process

AFM was performed on a Multimode 8 Atomic Force Microscope (Bruker) and recorded in PeakForce QNMmode. The solutions were obtained by dissolution of the polymers in a mixture of [Toluene : Propylene Glycol Methyl Ether Acetate (PGMEA)] [75 : 25], (2 wt%). The polymer films were obtained by spin-coating of a diluted polymer solution onto a silicon wafer at 2 krpm for 60 s. The sample was first characterised by AFM directly after spin-

coating and drying and then after annealing at 140°C for 30 minutes and subsequent quenching at room temperature.

3.5. Small-angle X-ray scattering (SAXS)

SAXS experiments were performed with a high-resolution X-ray spectrometer Xeuss 2.0 from Xenox. The spectrometer operates with a radiation wavelength of λ= 1.54 Å (Copper K_α radiation). Scattering patterns were collected using a PILATUS 300K Dectris detector with a sample-to-detector distance of 1637 mm. The collected data were analysed using Primus software. The film preparation for the SAXS experiment was done in a similar way as for the AFM characterization. The polymers were dissolved in a mixture of [Toluene : PGMEA] [75 : 25], (2wt%) and drop casted on a Kapton film. The films were annealed at 140°C for 30 minutes before analysis.

4. Results and discussion

4.1. Block copolymer synthesis

Poly(pentafluorostyrene-*b*-butyl acrylate) (PPFS-*b*-PBuA) block copolymers were synthesized by NMP controlled radical polymerization. The reaction was carried out by first synthetizing PPFS that was further used as a macro-initiator for the chain extension with BuA. PPFS homopolymers were characterized by ^{1}H NMR, SEC, and DSC. The backbone of PPFS are found to be located between 1.7 and 3 ppm (**Figure SI 1**). PPFS macro-initiators with molar masses ranging from 12 500 to 24 000 g/mol were obtained and their dispersity values ~~*Đ*~~ remained under 1.1 (**Table 1**). The glass transition temperature (*Tg*) of the PPFS homopolymer was determined to be around 100°C (**Figure SI 2**).

Acrylates were chosen for the BCP because they present properties such as flexibility, transparency, and toughness. [29] Moreover, poly(butyl acrylate) (PBuA) chemical atomic composition is different from poly(pentafluorostyrene)'s (PPFS), a suitable property to generate

a nano-phase separation by self-assembly. Indeed, for a phase separation to occur, the two blocks in the BCP must be non-miscible, property driven by their solubility parameters δ. The Hansen solubility parameters of the homopolymers PPFS and PBuA were calculated using HSPiP software and were of 16.1 $Mpa^{1/2}$ and 17.3 $Mpa^{1/2}$, respectively. Other systems of phase separation with a difference of solubility parameters have already been described in the literature. [30,31] As an example, the PS/PBuA (δ_{PS} = 18.4 $Mpa^{1/2}$) system is able to phase separate with a similar difference between solubility parameters than PPFS/PBuA system. [32]

As described previously, the morphologies of the nano-phase separation are dictated by the volume fraction Φ of one block. So, BCPs having different targeted molar ratios were synthesized to design different morphologies. To vary those molar ratios, different experimental parameters can be used as the conversion of the monomers through reaction time and monomer to macro-initiator ratio (**Table 1**). The molar compositions were calculated by ^{1}H NMR after purification of the BCPs. A typical ^{1}H NMR spectrum of PPFS-*b*-PBuA copolymer, with chemical shifts of the backbone protons of the copolymer (-CH and -CH_2) located between 1.8 and 2.9 ppm is represented in **Figure 1**. Protons of PBuA side chains, are located at 4 ppm (-OCH_2) and between 0.9 and 1.8 ppm for -CH_3 and -CH_2 ones. The final composition of each block in the BCP can then be determined by dividing the integral value of protons corresponding to one of the blocks with the integral value of the protons corresponding to the other block. An example of calculation is given in the supporting information to illustrate the procedure with $PPFS_{0.50}$-*b*-$PBuA_{0.50}$ (**Figure 1**, **Equation SI 1**).

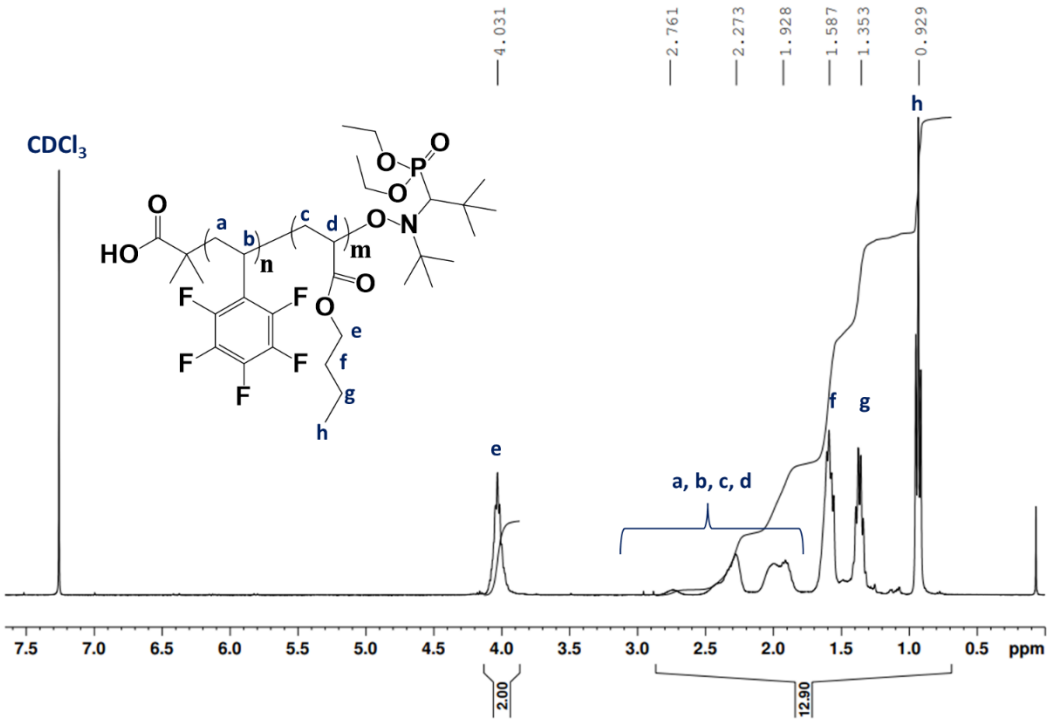

Figure 1. Schematic structure and ^{1}H NMR spectrum (300 MHz, room temperature, $CDCl_3$) of purified $(PPFS_{0.50}$-*b*-$PBuA_{0.50})_{34K}$ (BCP3).

The efficiency of the re-initiation of the PPFS was observed by DOSY NMR and SEC. DOSY NMR is a powerful characterization technique to determine the number of species existing in a complex solution, each being assessed by a diffusion coefficient. [33] Observing one diffusion coefficient means the presence of a unique species in the sample. For all PPFS-*b*-PBuA copolymers synthesized, only one diffusion coefficient is observed by DOSY NMR, which is characteristic of an efficient re-activation of the macro-initiator PPFS (**Figure SI 3**). SEC characterizations corroborate the good control over the polymerization (**Figure 2 A**). An increase in molar mass from homopolymers PPFS to PPFS-*b*-PBuA BCPs is attributed to the chain extension (**Figure 2**). Dispersity values $\mathit{Đ}$ between 1.09 and 1.88 are reported in **Table 1**. A dispersity value enhancement is noticed when the molar compositions of PBuA increases, with the apparition of a shoulder in the corresponding chromatograms corresponding to the highest molar mass of the macro-initiator PPFS (**Figure 2 A**, **Figure SI 4**). Such behaviour

could be attributed to non-reversible termination reactions which would lead to dead chains when the polymerization of the first block is pushed towards high conversion (here 85% for the PPFS macro-initiator).

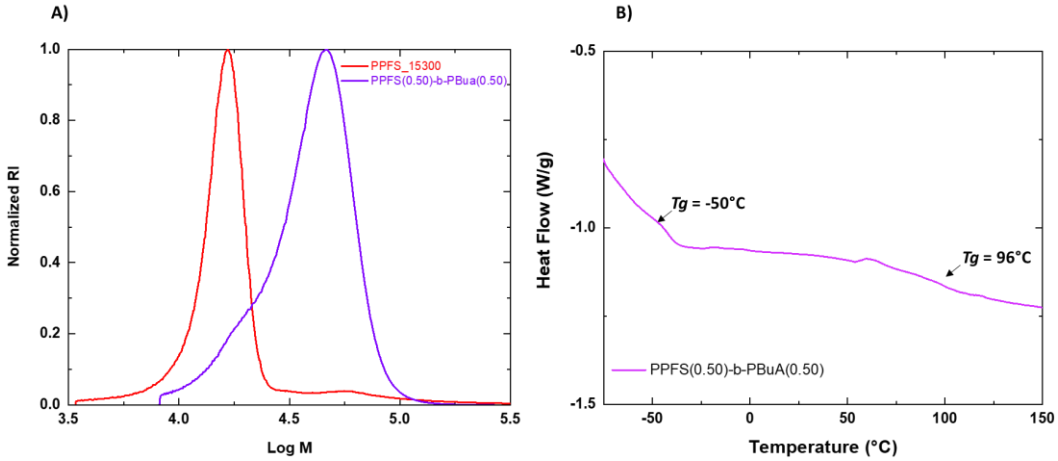

Figure 2. (A) SEC traces of poly(pentafluorostyrene) macro-initiator (PPFS3) (Mn = 15 300 g/mol, $Đ$ = 1.05) and the homologue $(PPFS_{0.50}\text{-}b\text{-}PBuA_{0.50})_{34K}$ (BCP3) (Mn = 34 000 g/mol, $Đ$ = 1.2). (B) DSC graph of BCP3 showing glass transition temperatures at -50°C and 96°C for PBuA and PPFS, respectively.

4.2. Block copolymers self-assembly

As previously mentioned, when BCPs are immiscible, they present the intrinsic properties of both isolated blocks. Thus, two glass transition temperatures *Tg*, at -50°C and 96°C, are noticeable on the BCP DSC thermogram for a PPFS/PBuA molar composition of 50/50 $(PPFS_{0.50}\text{-}b\text{-}PBuA_{0.50})_{34K}$ (here, the subscript 34K represents the molar mass of the copolymer obtained by SEC, the same notation was used for all the copolymers throughout the manuscript) (**Figure 2 B**). For the compositions with lower amount of PPFS, a different thermal pattern is observed with just the PBuA thermal transition. Indeed, the heat capacity Δ_{Cp} of PBuA is 3.8 times higher than the one of PPFS with values of -5.7 and -1.5 W/(kg.°C), respectively (**Figure SI 5**). BCPs self-assembly allows to design well-structured materials, when composed

of immiscible blocks. BCP systems will aim to minimize the interaction between blocks to reach a thermodynamic equilibrium. That microphase separation is induced by the stretching of the BCP chains with the desire of lowering interfacial energy in the BCP. The domains' structure is dictated by the volume fraction Φ of one block into the BCP. Depending on that volume fraction, the chains will stretch differently leading to different morphologies. [34,35] Typically, for the phase separation, the minor phase in volume will disperse in a matrix of the major one. Due to the strong interaction of the covalent bond linking the blocks, the phase separation can only occur at the macromolecular scale, meaning at the nanometre scale and not at the macroscopic one. [3] Moreover, domains size can be tuned by varying chains length N through the control of the molar mass.

Such nano-structured material based on the self-assembly behaviour of PPFS-*b*-PBuA BCPs can be observed at the scale length by Atomic Force Microscopy (AFM). To do so, solutions of each BCPs were prepared following the experimental section procedure. The solutions were then spin coated on silicon wafers. A thermal annealing of the films was done at 140°C to reach the thermodynamic equilibrium (40° higher than the *Tg* of PPFS). Each sample was observed before and after annealing. The AFM results on thin films were correlated with bulk study by Small Angle X-rays Scattering SAXS. Indeed, the SAXS experiment will complement the information provided by AFM measurements and give detailed insight on the arrangement of the microstructures in the bulk (films of few hundred microns thick) and their domains size. If periodic structural structuration occurs, the SAXS pattern will reveal the presence of specific maxima of scattering intensities at different scattering vectors (q). The ratio between a given q and the maxima value of q in intensity (q^*) will provide information about the spacing between nanodomains, and the type of structuration in the material. [36]

Taking $(PPFS_{0.50}\text{-}b\text{-}PBuA_{0.50})_{34K}$ (BCP3) as an example, the molar composition of each block is 0.5, leading to a volume fraction Φ of 0.60 and 0.40 for PPFS and PBuA, respectively

(ρ_{PFS} = 1.4 g/mL; ρ_{BuA} = 1.08 g/mL). According to the theoretical BCP phase diagram, [34] the equilibrium morphology expected at this volume fraction is to be determined by lamellas (LAM), which was experimentally observed by AFM and SAXS (**Figure 3**) with an average spacing between nanodomains of 35 nm. The calculation of the spacing is provided in the supporting information (**Equation SI 4**).

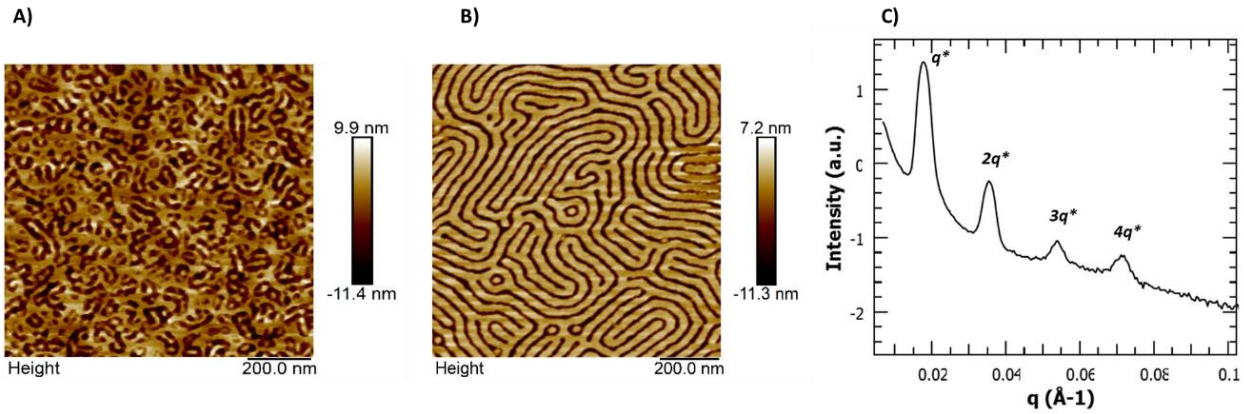

Figure 3. (A) Peak Force mode AFM height images of $PPFS_{0.50}$-*b*-$PBuA_{0.50}$ (BCP3) film before annealing and (B) after annealing at 140°C for 4 hours; (C) Observation of the annealed film by SAXS.

Similarly, for the other compositions the samples were annealed before AFM observation following the procedure described in the experimental section of this article. The volume fraction of each block was determined and the BCPs were observed by AFM and SAXS. Different morphologies were observed with distance between nanodomains ranging from 30 to 45 nm (**Table 1**). The results are shown in **Figure 4**, where are presented for each composition the AFM images and corresponding SAXS results. As it was expected from the self-assembly theory, composition $(PPFS_{0.90}$-*b*-$PBuA_{0.10})_{17K}$ (BCP6) gave no self-assembly both by AFM and SAXS, and the remaining BCPs were proven to self-assemble both by AFM and SAXS, giving a hexagonal closed-packed cylinders HCC structuration.

Table 1. Summary table of block copolymer synthesis and characterizations.

BCPs	Polymer $PPFS_x$-*b*-$PBuA_y$*	$\frac{[monomer]}{[initiator]}$	BuA Conv[b] (%)	M_n[a] (g/mol) Eq PS (M_n^{theo})	M_w[a] (g/mol) Eq PS	$Đ$[a]	Degree of Polymerization (DP_n)		f_v (PPFS)	f_v (PBuA)	T_g[c] (°C)	Structure by SAXS & AFM[d, e]	Pitch by SAXS[d] (nm)
							PPFS	PBuA					
BCP1[f]	$PPFS_{0.16}$-*b*-$PBuA_{0.84}$	414	69	31 000 (56 000)	38 800	1.26	65	340	0.18	0.82	-39	HCC	45
BCP2[g]	$PPFS_{0.33}$-*b*-$PBuA_{0.67}$	546	14	40 100 (34 000)	75 700	1.88	73	155	0.37	0.63	-40 / 104	HCC	45
BCP3[h]	$PPFS_{0.50}$-*b*-$PBuA_{0.50}$	483	12	34 000 (25 000)	42 000	1.2	79	79	0.54	0.46	-50 / 96	LAM	35
BCP4[f]	$PPFS_{0.54}$-*b*-$PBuA_{0.46}$	227	15	37 000 (19 000)	50 600	1.36	65	50	0.58	0.42	-39	HCC	46
BCP5[i]	$PPFS_{0.86}$-*b*-$PBuA_{0.14}$	195	15	30 600 (27 000)	34 400	1.12	125	19	0.88	0.12	103	HCC	28
BCP6[f]	$PPFS_{0.90}$-*b*-$PBuA_{0.10}$	97	2	17 400 (14 000)	19 100	1.09	65	8	0.91	0.09	-	Disorder	-

*With x = molar % of PPFS and y = molar % of PBuA.

[a] Determined by SEC by equivalent PS, [b] Determined by ^1H NMR (300 MHz, room temperature, $CDCl_3$), *[c] DSC, [d] SAXS & [e] AFM.*

BCPs synthetized from macro-initiators: [f] (PPFS1) (Mn = 12 500 g/mol, Mw = 13 400 g/mol, $Đ$ = 1.07), [g] (PPFS2) (Mn = 14 100 g/mol, Mw = 15 200 g/mol, $Đ$ = 1.07), [h] (PPFS3) (Mn = 15 300 g/mol, Mw = 16 100 g/mol, $Đ$ = 1.05), [i] (PPFS4) (Mn = 24 000 g/mol, Mw = 26 400 g/mol, $Đ$ = 1.1).

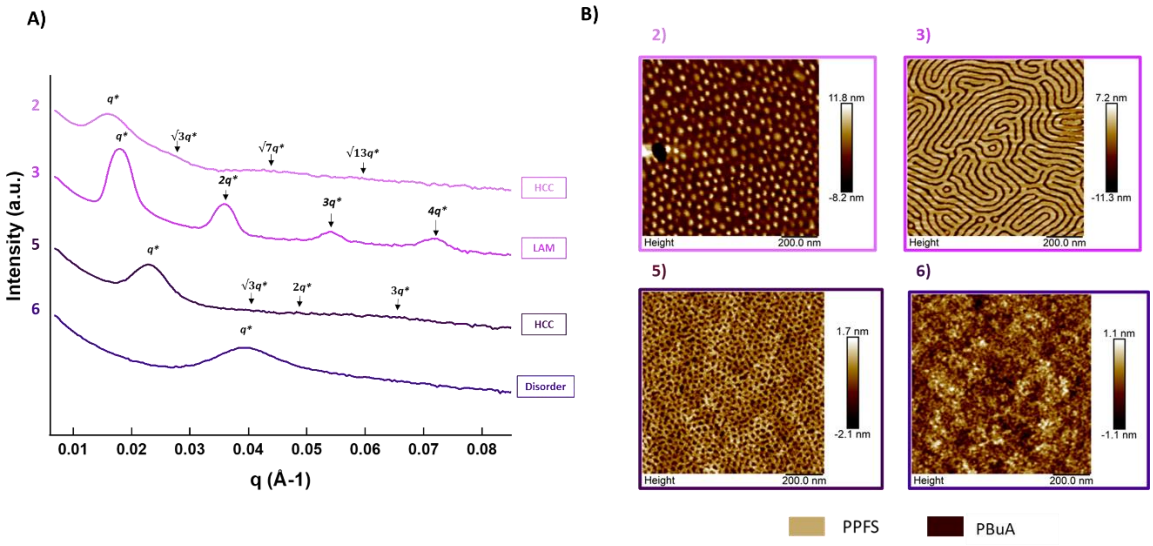

Figure 4. (A) SAXS graph of the different block copolymers after annealing at 140°C for 3h. (B) Peak Force mode AFM height images of PPFS-*b*-PBuA BCPs after annealing at 140°C for 4 h. (BCP2~2) $(PPFS_{0.33}\text{-}b\text{-}PBuA_{0.67})_{40K}$; (BCP3~3) $(PPFS_{0.50}\text{-}b\text{-}PBuA_{0.50})_{34K}$; (BCP5~5) $(PPFS_{0.86}\text{-}b\text{-}PBuA_{0.14})_{31K}$; (BCP6~6) $(PPFS_{0.90}\text{-}b\text{-}PBuA_{0.10})_{17K}$).

4.3. Driven self-assembly of block copolymers

The morphology of the BCPs can be modified by addition of a defined amount of homopolymer in the blend. The idea is to mimic the presence of dead PPFS chains which could be present in the final block copolymers and then perturb the self-assembly pattern. In order to check the impact of residual macro-nitiator, 10 wt% of PPFS1 homopolymer of a molar mass of 12 500 g/mol with $\cancel{D}$ of 1.07 (DPn = 65) was added to BCP1 and BCP4, respectively $(PPFS_{0.16}\text{-}b\text{-}PBuA_{0.84})_{31K}$ and $(PPFS_{0.54}\text{-}b\text{-}PBuA_{0.46})_{37K}$. By doing so, the overall molar composition of PPFS is increased, leading to an enrichment of the PPFS phase, giving respectively $PPFS_{0.24}\text{-}b\text{-}PBuA_{0.76}$ (BCP1') and $PPFS_{0.59}\text{-}b\text{-}PBuA_{0.41}$ (BCP4'). Hence a shift from the lower to higher volume fraction in PPFS in the BCP phase diagram is expected. On top of modifying the composition of the PPFS block, adding some homopolymer of PPFS in the blend has an influence on the self-assembly and nano-pattern of the material. In the case of

BCP1 ($PPFS_{0.16}$-*b*-$PBuA_{0.84}$)$_{31K}$, enriching the PPFS phase provided a better phase separation with well-defined nanodomains. Moreover, the SAXS analysis reveals a cubic structuration and a pitch distance decreasing from 45 to 38 nm. For BCP4 ($PPFS_{0.54}$-*b*-$PBuA_{0.46}$)$_{37K}$, two hypotheses could explain the contrast observed on the AFM images after addition of PPFS homopolymer (**Figure 5 A & B** - BCP4 to BCP4'). Indeed, nanodomains of PBuA in a PPFS matrix are expected by AFM. However, this new composition displays the opposite result, *i.e.* nanodomains of PPFS in PBuA matrix (**Figure 5 A** - BCP4'). The first explanation could be that the nanodomains of the initial composition (**Figure 5 A** - BCP4) were mainly parallel to the surface of the film, *i.e. in-plane*, and they became perpendicular to it after addition of PPFS, *i.e. out-of-the plane*. The second explanation could be a metastable state of the copolymer, called HPL (Hexagonally Perforated Lamellae). Such structuration corresponds to lamellas of the minor PBuA polymer being covered by hexagonal arrangement of perforations. [37] This structure can be the result of the presence of chains of different length, *i.e.* dispersity value ~~*Đ*~~ of 1.36 plus free homopolymer PPFS. [37,34] Nevertheless, the pitch distance of 45 nm remained the same after addition of PPFS. Here, we demonstrated a way to drive the morphologies of PPFS-*b*-PBuA BCPs by adding a defined amount of homopolymer.

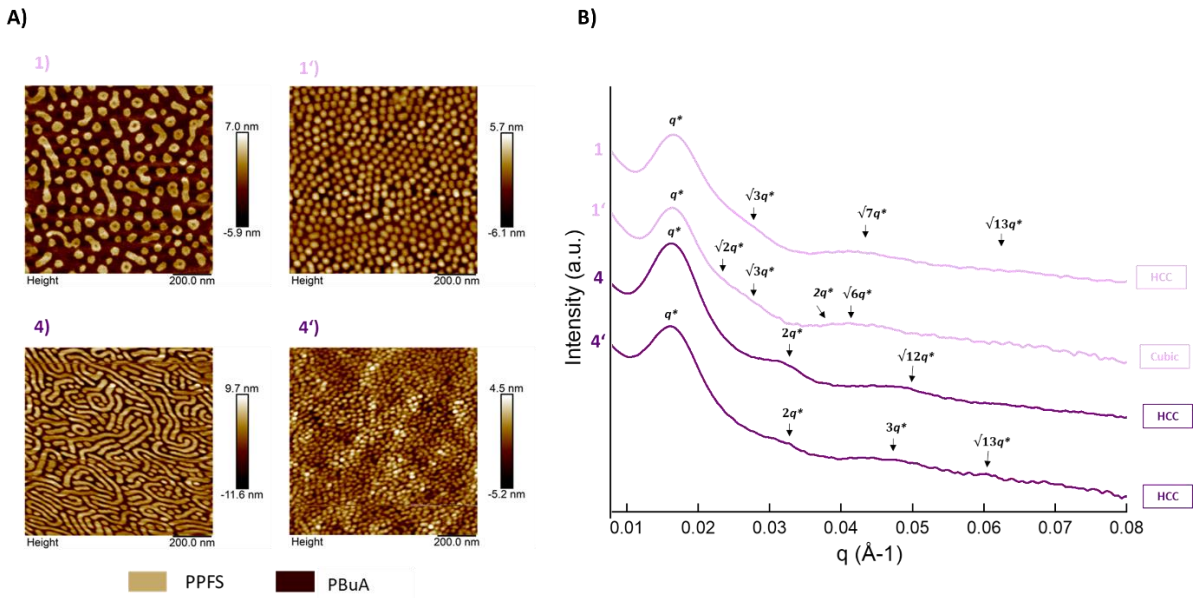

Figure 5. (A) AFM of the original and tuned BCPs annealed at 140°C for 4 h. Tunability of the morphology observed by adding 10 wt% of $PPFS_{12500}$ in BCP mixtures; shift of the molar composition of BCP1~1 ($PPFS_{0.16}$-*b*-$PBuA_{0.84}$) and BCP4~4 ($PPFS_{0.54}$-*b*-$PBuA_{0.46}$) after addition of PPFS1 to give BCP1'~1' ($PPFS_{0.24}$-*b*-$PBuA_{0.76}$) and BCP4'~4' ($PPFS_{0.59}$-*b*-$PBuA_{0.41}$) depending on the molar fraction of PPFS on a theoretical BCP phase diagram. (B) SAXS of the original and tuned BCPs annealed at 140°C for 3h.

As mentioned previously, the substitution of the fluorine in *para*-position allows for many possibilities of functionalization permitting to tune either the volume fraction or the interaction parameter χ which is dependant of the difference of the solubility parameters δ of the two blocks of the modified BCP3 ($(PPFS_{0.33}$-*b*-$PBuA_{0.67})_{40K}$). Here, the *para* fluorine-thiol modification was performed as an efficient soft substitution with a functional thiol, *i.e.* 1-hexanethiol compound, in a one-step organo-catalyzed procedure with 1,8-Diazabicyclo[5.4.0]undec-7-ene DBU. Indeed, mild conditions at room temperature and ambient atmosphere were used. Moreover, the versatility and the commercial availability of thiol compounds make them attractive for such reactions. [38] The reaction was performed in DMF overnight at room temperature. The modified BCP was characterized by ^{19}F NMR (**Figure 6**). On the NMR spectrum, the full efficiency of the substitution is characterized by the complete disappearance of the chemical shift of the fluorine in *para* position (δ_{paraF} = -154 ppm). Moreover, the chemical up fields shift of the fluorine in *meta* positions is also observed from δ_{metaF} = -161 to 134 ppm, before and after modifications, respectively. This up field shift is due to the change from fluorine to sulphur neighbours.

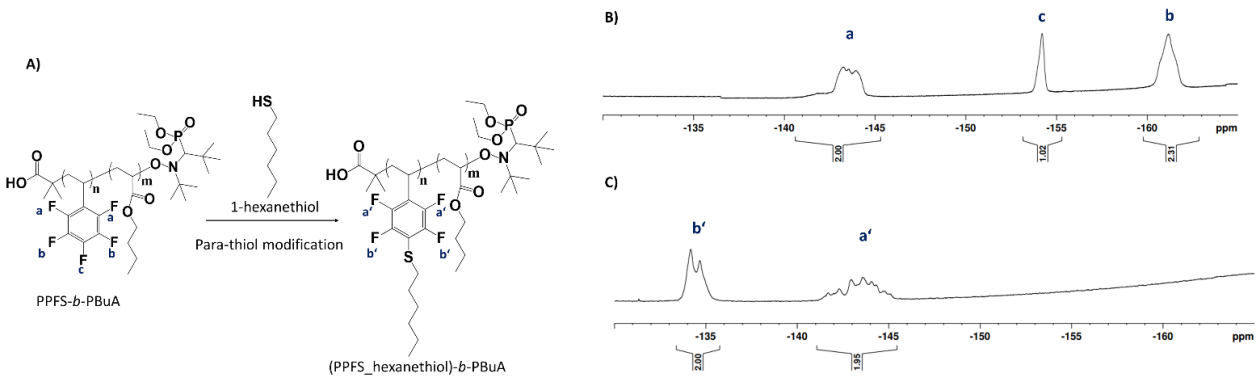

Figure 6. (A) Polymer structure before and after modification, (B) ^{19}F NMR spectra of BCP3 $(PPFS_{0.33}\text{-}b\text{-}PBuA_{0.67})_{40K}$ (300 MHz, room temperature, $CDCl_3$) and (C) BCP3 after modification with 1-hexanethiol (300 MHz, room temperature, $CDCl_3$).

After full modification of the BCP, the glass transition temperature *Tg* of the PPFS block is expected to be lowered due to the added side chain providing additional free volume and then mobility to the polymer chains. Indeed, the *Tg* of the 1-hexanethiol modified PPFS drops down to 11°C and the macroscopic aspect of the polymer changed from solid to viscous at room temperature after modification (**Figures SI 6 & 7**).

The AFM images of the modified BCP do not show a contrasted image after modification. This can be explained by the new solubility parameter of the 1-hexanethiol modified PPFS (17.4 $Mpa^{1/2}$), which is close to the one of PBuA (17.3 $Mpa^{1/2}$). This proximity of the solubility parameters strongly decreased the segregation ability along with similar thermal behaviours, *i.e.* both in an elastomeric state with *Tg* values below room temperature. Here, the modification with 1-hexanethiol did not preserve the nano-segregation of the initial self-assembled block copolymer (**Figure 8**). This observation was confirmed by the SAXS experiment. Indeed, no other than the initial scattering vector q^* at 0.017 $Å^{-1}$ were observed, characteristic of a liquid order.

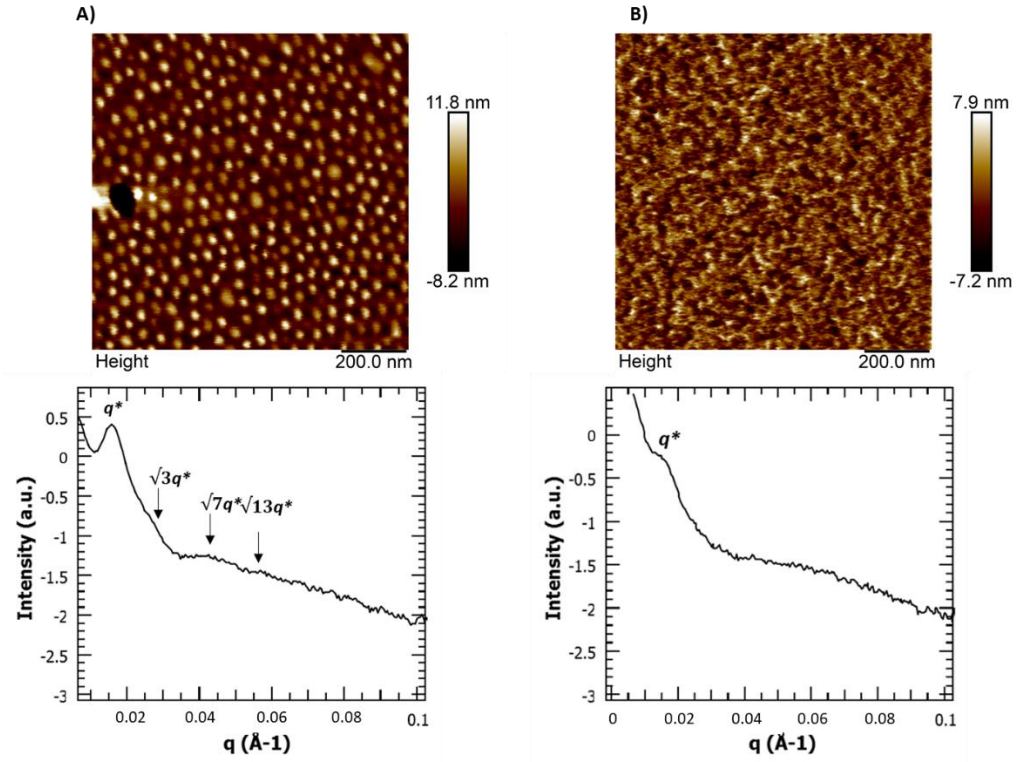

Figure 8. (A) Peak Force mode AFM height images and corresponding SAXS characterizations of BCP3 ($PPFS_{0.33}$-*b*-$PBuA_{0.67})_{40K}$, and (B) BCP3 modified with 1-hexanethiol after annealing.

5. Conclusion

In the present study, the synthesis and self-assembly behaviour of PPFS-*b*-PBuA block copolymers were studied. The synthesis of the BCPs was performed by NMP controlled radical polymerization from PPFS macroinitiator by the chain extension with butyl acrylate BuA. BCPs of PPFS with molar fraction ranging from 0.16 to 0.90 were synthesized. The molar masses of the PPFS-*b*-PBuA BCPs were determined by SEC between 17 000 and 40 000 g/mol with dispersity values *Đ* between 1.07 and 1.88. The chromatograms showed an increase in molar mass due to the chain extension from the macro-initiator to the BCPs and a single diffusion coefficient by DOSY NMR.

Two glass transition temperatures *Tg* were observed by DSC for the block copolymers. The self-assembly behaviour of the PPFS-*b*-PBuA was brought to light by AFM observation

on thin films correlated to SAXS analysis in bulk. Indeed, depending on the volume fraction of each block, the morphologies obtained were tuned from HCC to LAM. The size of the nanodomains was between 30 and 45 nm. Moreover, morphologies could also be varied by addition of 10% of PPFS homopolymer to the BCP blend.

Finally, the BCPs were modified by *para* fluorine-thiol modification using 1-hexanethiol. The full modification of the PPFS block was determined by ^{19}F NMR and a change in thermal properties of the BCP was noticeable after modification with 1-hexanethiol.

The *para* fluorine-thiol modification can be finally considered as an easy mild and efficient organo-catalyzed method for the tailoring of functional block polymers microstructure in relationship with their physical or chemical properties due to the variety of available thiol functional side chains. Moreover, this method's added feature represents an important way to pave the development of nano-structured materials for different applications fields, as energy, especially. Indeed, by controlling the solubility parameter of the modified PPFS block and then maintaining it different enough of the second block one, the degree nano-segregation can be tuned.

Corresponding Authors:

e-mail: laurent.billon@univ-pau.fr

Acknowledgements.

This work was realized in the framework of the ITN EJD eSCALED project. The eSCALED project has received funding from the European Union's Horizon 2020 research and innovation program under grant agreement No. 765376. PM thanks ES2 UPPA ENSUITE Project for his fellow.

The authors would like to thank Ahmed Bentaleb of the *Centre de Recherche Paul Pascal* (CRPP) in Bordeaux for the SAXS experiments.

References

[1] V.F. Cardoso, D.M. Correia, C. Ribeiro, M.M. Fernandes, S. Lanceros-Méndez, Fluorinated polymers as smart materials for advanced biomedical applications, *Polymers* **10** (2018) 1–26. https://doi.org/10.3390/polym10020161.

[2] D.R. Iyengar, S.M. Perutz, C.A. Dai, C.K. Ober, E.J. Kramer, Surface segregation studies of fluorine-containing diblock copolymers, *Macromolecules* **29** (1996) 1229–1234. https://doi.org/10.1021/ma950544z.

[3] Y. Mai, A. Eisenberg, Self-assembly of block copolymers, *Chem. Soc. Rev.* **41** (2012) 5969–5985. https://doi.org/10.1039/C2CS35115C.

[4] A. Rösler, G.W.M. Vandermeulen, H.A. Klok, Advanced drug delivery devices via self-assembly of amphiphilic block copolymers, *Adv. Drug Deliv. Rev.* **64** (2012) 270–279. http://dx.doi.org/10.1016/j.addr.2012.09.026.

[5] V. Agrahari, Advances and applications of block-copolymer-based nanoformulations, *Drug Discov. Today* **23** (2018) 1139–1151.https://doi.org/10.1016/j.drudis.2018.03.004.

[6] A. Lendlein, S. Kelch, Shape-Memory Polymers, *Angew. Chem. Int. Ed. Engl.* **41** (2002) 2034–2057.https://doi.org/10.1002/1521-3773(20020617)41:12%3C2034::AID-ANIE2034%3E3.0.CO;2-M.

[7] R.A. Puglisi, Towards Ordered Silicon Nanostructures through Self-Assembling Mechanisms and Processes, *J. Nanomater.* **2015** (2015) 1-20. https://doi.org/10.1155/2015/586458.

[8] W. Lu, Y. Wang, W. Wang, S. Cheng, J. Zhu, Y. Xu, K. Hong, N-G. Kang, J. Mays, All Acrylic-based Thermoplastic Elastomers with High Upper Service Temperature and Superior Mechanical Properties, *Polym. Chem.* **8** (2017) 5741–5748. https://doi.org/10.1039/C7PY01225J.

[9] D. Benoit, S. Grimaldi, J.P. Finet, P. Tordo, M. Fontanille, Y. Gnanou, Controlled/Living

Free-Radical Polymerization of Styrene and n-Butyl Acrylate in the Presence of a Novel Asymmetric Nitroxyl Radical, *ACS Symp. Ser.* **685** (1998) 225–235. DOI: 10.1021/bk-1998-0685.ch014.

[10] J. Chiefari, Y.K. Chong, F. Ercole, J. Krstina, J. Jeffery, T.P.T. Le, R.T.A. Mayadunne, G.F. Meijs, C.L. Moad, G. Moad, E. Rizzardo, S.H. Thang, Living Free-Radical Polymerization by Reversible Addition - Fragmentation Chain Transfer : The RAFT Process, *Macromolecules* **31** (1998) 5559–5562. https://doi.org/10.1021/ma9804951.

[11] K. Matyjaszewski, Atom Transfer Radical Polymerization (ATRP): Current status and Future Perspectives, *Macromolecules* **45** (2012) 4015–4039. https://doi.org/10.1021/ma3001719.

[12.] J. Nicolas, Y. Guillaneuf, C. Lefay, D. Bertin, D. Gigmes, B. Charleux, Nitroxide-mediated polymerization, *Prog. Polym. Sci.* **38** (2005) 63-235. http://dx.doi.org/10.1016/j.progpolymsci.2012.06.002.

[13] K. Matyjaszewski, J. Xia, Atom Transfer Radical Polymerization, *Chem. Rev.* **101** (2001) 2921–2990. https://doi.org/10.1021/cr940534g.

[14] G. Moad, E. Rizzardo, S.H. Thang, Living Radical Polymerization by the RAFT Process, *Aust. J. Chem.* **58** (2005) 379–410. https://doi.org/10.1071/CH05072.

[15] T.L. Bucholz, S.P. Li, Y.L. Loo, Ultra-low-κ materials derived from poly(D,L-lactide-*b*- pentafluorostyrene) diblock copolymers, *J. Mater. Chem.* **18** (2008) 530–536. https://doi.org/10.1039/B714941G.

[16] K. Jankova, P. Jannasch, S. Hvilsted, Ion conducting solid polymer electrolytes based on polypentafluorostyrene-*b*-polyether-*b*-polypentafluorostyrene prepared by atom transfer radical polymerization, *J. Mater. Chem.* **14** (2004) 2902–2908. https://doi.org/10.1039/B404097J.

[17] X. Li, L. Andruzzi, E. Chiellini, G. Galli, C.K. Ober, A. Hexemer, E.J. Kramer, D.A.

Fischer, Semifluorinated Aromatic Side-Group Polystyrene-Based Block Copolymers: Bulk Structure and Surface Orientation Studies, *Macromolecules* **35** (2002) 8078–8087. https://doi.org/10.1021/ma020463k.

[18] S. Chen, A. Funtan, F. Gao, B. Cui, A. Meister, S.S.P. Parkin, W.H. Binder, Synthesis and Morphology of Semifluorinated Polymeric Ionic Liquids, *Macromolecules* **51** (2018) 8620–8628. https://doi.org/10.1021/acs.macromol.8b01624.

[19] K.T. Powell, C. Cheng, K.L. Wooley, Complex Amphiphilic Hyperbranched Fluoropolymers by Atom Transfer Radical Self-Condensing Vinyl (Co)polymerization, *Macromolecules* **40** (2007) 4509–4515. https://doi.org/10.1021/ma0628937.

[20] S. Borkar, K. Jankova, H.W. Siesler, S. Hvilsted, New Highly Fluorinated Styrene-Based Materials with Low Surface Energy Prepared by ATRP, *Macromolecules* **37** (2004) 788–794. https://doi.org/10.1021/ma034952b.

[21] Q. Yin, A. Charlot, D. Portinha, E. Beyou, Nitroxide-mediated polymerization of pentafluorostyrene initiated by PS-DEPN through the surface of APTMS modified fumed silica: Towards functional nanohybrids, *RSC Adv.* **6** (2016) 58260–58267. DOI: 10.1039/c6ra08973a.

[22] C.R. Becer, K. Babiuch, D. Pilz, S. Hornig, T. Heinze, M. Gottschaldt, U.S. Schubert, Clicking Pentafluorostyrene Copolymers: Synthesis, Nanoprecipitation, and Glycosylation, *Macromolecules* **42** (2009) 2387–2394. https://doi.org/10.1021/ma9000176.

[23] C. Ott, R. Hoogenboom, U.S. Schubert, Post-modification of poly(pentafluorostyrene): a versatile "click" method to create well-defined multifunctional graft copolymers, *Chem. Commun.* (2008) 3516–3518. https://doi.org/10.1039/B807152G.

[24] C.S. Gudipati, M.B.H. Tan, H. Hussain, Y. Liu, C. He, T.P. Davis, Synthesis of Poly(glycidyl methacrylate)-*block*-Poly(pentafluorostyrene) by RAFT: Precursor to

Novel Amphiphilic Poly(glyceryl methacrylate)-*block*-Poly(pentafluorostyrene), *Macromol. Rapid Commun.* **29** (2008) 1902–1907. https://doi.org/10.1002/marc.200800515.

[25] J.M. Noy, Y. Li, W. Smolan, P.J. Roth, Azide-*para*-Fluoro Substitution on Polymers: Multipurpose Precursors for Efficient Sequential Postpolymerization Modification, *Macromolecules* **52** (2019) 3083–3091. https://doi.org/10.1021/acs.macromol.9b00109.

[26] L. Dumas, E. Fleury, D. Portinha, Wettability adjustment of PVDF surfaces by combining radiation-induced grafting of (2,3,4,5,6)-pentafluorostyrene and subsequent chemoselective "click-type" reaction, *Polymer* **55** (2014) 2628–2634. http://dx.doi.org/10.1016/j.polymer.2014.04.002.

[27] Q. Yin, P. Alcouffe, E. Beyou, A. Charlot, D. Portinha, Controlled perfluorination of poly(2,3,4,5,6-pentafluorostyrene) (PPFS) and PPFS-functionalized fumed silica by thiol-*para*-fluoro coupling: Towards the design of self-cleaning (nano)composite films, *Eur. Polym. J.* **102** (2018) 120–129. https://doi.org/10.1016/j.eurpolymj.2018.03.016.

[28] M. Riedel, J. Stadermann, H. Komber, F. Simon, B. Voit, Synthesis, post-modification and self-assembled thin films of pentafluorostyrene containing block copolymers, *Eur. Polym. J.* **47** (2011) 675–684. http://dx.doi.org/10.1016/j.eurpolymj.2010.10.010.

[29] A. Serrano-Aroca, S. Deb, *Acrylate Polym. Adv. Appl.* (2019). DOI:10.5772/intechopen.77563.

[30] P. Marcasuzaa, M. Save, P. Gérard, L. Billon, When a pH-triggered nanopatterned shape transition drives the wettability of a hierarchically self-organized film: A bio-inspired effect of “sea Anemone”, *J. Colloid Interface Sci.* **581** (2021) 96–101. https://doi.org/10.1016/j.jcis.2020.07.130.

[31] P. Marcasuzaa, S. Pearson, K. Bosson, L. Pessoni, J-C. Dupin, L. Billon, Reactive nano-patterns in triple structured bio-inspired honeycomb films as a clickable platform, *Chem.*

Commun. **54** (2018) 13068–13071. https://doi.org/10.1039/C8CC05333B.

[32] P. Escalé, M. Save, L. Billon, J. Ruokolainen, L. Rubatat, When block copolymer self-assembly in hierarchically ordered honeycomb films depicts the breath figure process, *Soft Matter* **12** (2016) 790–797. https://doi.org/10.1039/C5SM01774B.

[33] N. Cherifi, A. Khoukh, A. Benaboura, L. Billon, Diffusion-Ordered Spectroscopy NMR DOSY: An All-In-One Tool to Simultaneously Follow Side Seactions, Livingness and Molar Masses of PolyMethylMethacrylate by Nitroxide Mediated Polymerization, *Polym. Chem.* **7** (2016) 5249–5257. https://doi.org/10.1039/C6PY00927A.

[34] M.W. Matsen, F.S. Bates, Unifying Weak- and Strong-Segregation Block copolymer Theories, *Macromolecules* **29** (1996) 1091–1098. https://doi.org/10.1021/ma951138i.

[35] L. Leibler, Theory of Microphase Separation in Block copolymers, *Macromolecules* **13** (1980) 1602–1617. https://doi.org/10.1021/ma60078a047.

[36] M. Zhang, R.B. Moore, T.E. Long, J.S. Riffle, Morphological Characterization and Analysis of Ion- Containing Polymers Using Small Angle X-ray Scattering Morphological Characterization and Analysis of Ion-Containing Polymers Using Small Angle X-ray Scattering, 2014.

[37] J. Listak, W. Jakubowski, L. Mueller, A. Plichta, K. Matyjaszewski, M.R. Bockstaller, Effect of Symmetry of Molecular Weight Distribution in Block Copolymers on Formation of "Metastable" Morphologies, *Macromolecules* **41** (2008) 5919–5927. https://doi.org/10.1021/ma800816j.

[38] G. Delaittre, L. Barner, The: *para*-Fluoro-Thiol Reaction as an Efficient Tool in Polymer Chemistry, *Polym. Chem.* **9** (2018) 2679–2684. https://doi.org/10.1039/C8PY00287H.

Supporting Information

PentaFluoroStyrene-based Block Copolymers Controlled Self-Assembly Pattern: a platform paving the way to functional structured polymers

Karell Bosson,[1,2,3] Pierre Marcasuzaa,[1,2] Antoine Bousquet,[2] Vladimir Atanasov,[3] Günter E.M. Tovar,[4,5] Laurent Billon[1, 2]

[1] Bio-inspired Materials Group: Functionalities & Self-assembly, E2S UPPA, 64000 Pau, France

[2] Universite de Pau et Pays de l'Adour, E2S UPPA, CNRS, IPREM, UMR5254, 64000 Pau, France

[3] Institute of Chemical Process Engineering, University of Stuttgart, Stuttgart, Germany

[4] Institute for Interfacial Process Engineering and Plasma Technology IGVP, University of Stuttgart, Pfaffenwaldring 31, 70569 Stuttgart, Germany

[5] Fraunhofer Institute for Interfacial Engineering and Biotechnology IGB, Nobelstr. 12, 70569 Stuttgart, Germany

This supporting information contains:

-Total number of pages: **11 pages**

-Total number of figures: **7 figures**

^{1}H NMR, DOSY NMR, SEC, DSC of the block copolymers and modified block copolymer used in this work

-Total number of Equations: **4 Equations**

Equations used to determine the molar compositions of the BCPs, the molar mass and volume fractions of the BCPs; and the pitch between nanodomains by SAXS

-Total number of Tables: **1 Table**

SAXS data of the copolymers described in this work

The supporting information of this article provides additional information on the synthesis and characterizations of the polymers. Here are presented the methodology for the calculations of polymer compositions, theoretical molar masses, distance between nanodomains for the SAXS analysis.

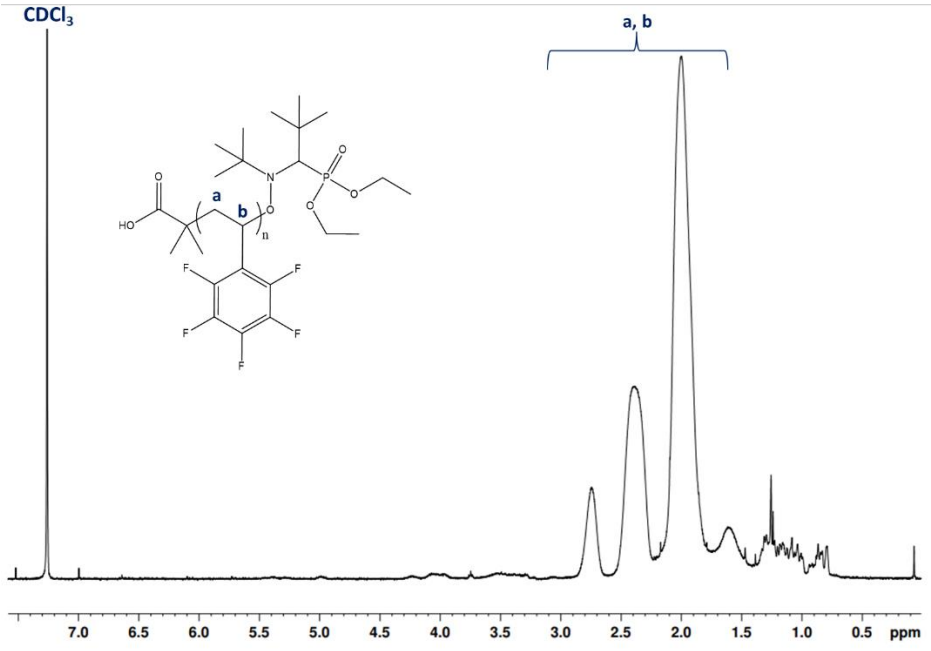

Figure SI 1. Structure and ^{1}H NMR spectrum (300 MHz, room temperature, $CDCl_3$) of poly(pentafluorostyrene) macro-initiator (PPFS2).

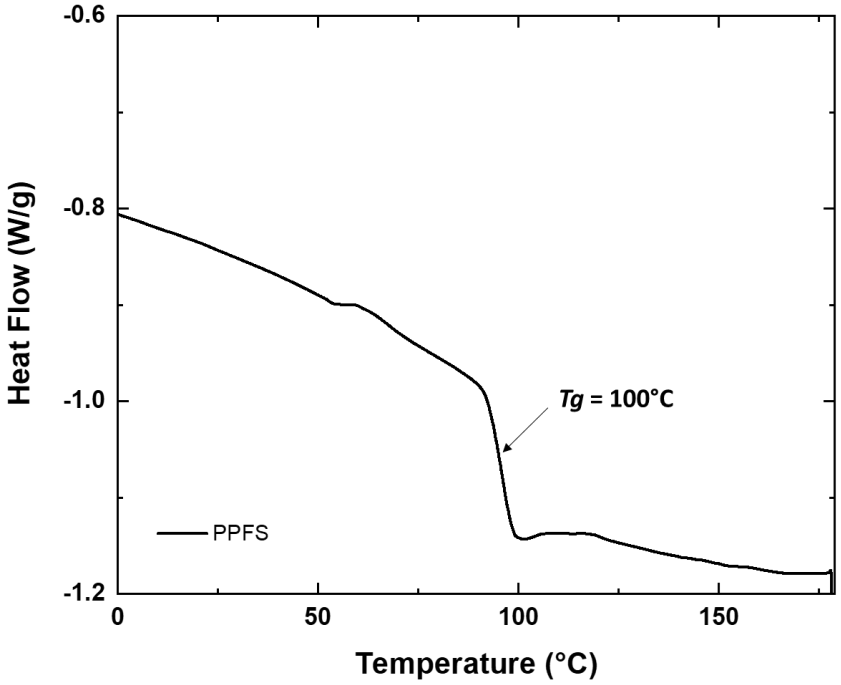

Figure SI 2. DSC of poly(pentafluorostyrene) macro-initiator (PPFS2), displaying a *Tg* of 100°C.

- Determining composition and volume fraction of PPFS and PBuA in the BCP

Like for the previous example, the attribution of the signals of each proton of the BCP was made, followed by the integration of those signals. The chemical shifts of the backbone protons of the copolymer (-CH and -CH_2) are located between 1.8 and 2.9 ppm ($Integral_{H\ PPFS}$ and $Integral_{H\ PBuA}$). Protons of PBuA side chains (-CH_3 and -CH_2) are located between 0.9 and 1.8 ppm and -OCH_2 protons of the PBuA side chain are situated at 4 ppm ($Integral_{H\ PBuA}$) (**Figure 1**). After calculation using the equation below, the molar composition of each block is of 0.50.

Equation SI 1. Molar composition of PPFS and PBuA in the BCP.

$$\%PBuA = [(Integral_{1H\ PBuA}) / (Integral_{1H\ PPFS} + Integral_{1H\ PBuA})] \times 100$$

$$\%PPFS = 100 - \%PBuA$$

$$\%PBua = \frac{\text{Integral}_{1H\ PBua}}{\text{Integral}_{1H\ PPFS} + \text{Integral}_{1H\ PBua}} \times 100$$

$$\%PPFS = 100 - \%PBua$$

Equation SI 2. Volume fraction of PPFS and PBuA in the BCP.

$$Ø_{PBuA} = [(MW_{PBuA} / \rho_{BuA})] / [(MW_{PPFS} / \rho_{PFS}) + (MW_{PBuA} / \rho_{BuA})]$$

$$Ø_{PPFS} = 1 - Ø_{PBuA}$$

$$Ø_{PBua} = \frac{\frac{MW_{PBua}}{\rho_{Bua}}}{\frac{MW_{PPFS}}{\rho_{PFS}} + \frac{MW_{PBua}}{\rho_{Bua}}}$$

$$Ø_{PPFS} = 1 - Ø_{PBua}$$

Where ρ_{PFS} = 1.4 g/mL and ρ_{BuA} = 1.08 g/mL

- Theoretical molar mass:

The theoretical molar mass (MW) of the block copolymers is determined using the conversion obtained by ^{1}H NMR. Considering PFS as monomer A and BuA as monomer B, the theoretical molar mass of the BCPs is:

Equation SI 3. Theoretical determination of the molar mass of the BCPs.

$$MW_{poly\ Btheo} = MW_{BlocBuilder} + \{[(\text{molar composition}_{\text{monomer A}} \times \text{Conversion}_{A}) / \text{molar composition}_{\text{initiator}}] \times M_{\text{monomer A}}\} + \{[(\text{molar composition}_{\text{monomer B}} \times \text{Conversion}_{B}) / \text{molar composition}_{\text{initiator}}] \times M_{\text{monomer B}}\}$$

$$MW_{poly\ B_{theo.}} = MW_{BlocBuilder} + \left[\frac{molar\ composition_{monomer\ A} \times Conversion_{A}}{molar\ composition_{initiator}}\right] \times M_{monomer\ A} + \left[\frac{molar\ composition_{monomer\ B} \times Conversion_{B}}{molar\ composition_{initiator}}\right] \times M_{monomer\ B}$$

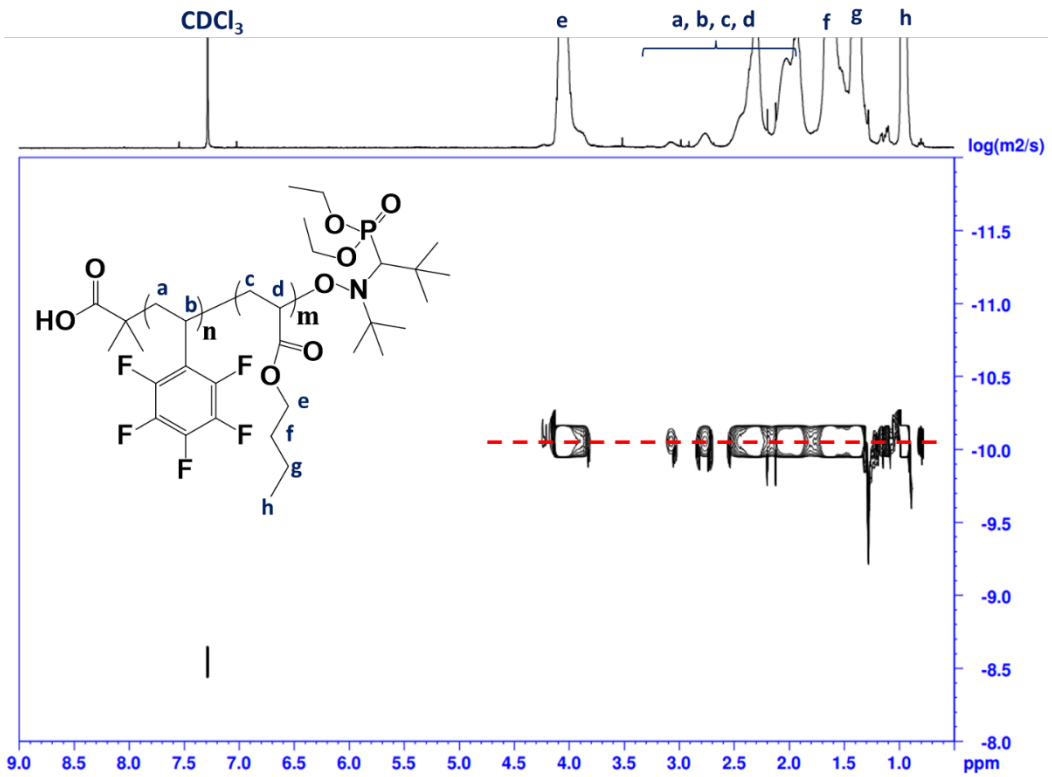

Figure SI 3. Structure and DOSY NMR spectrum (300 MHz, room temperature, $CDCl_3$) of purified $(PPFS_{0.54}\text{-}b\text{-}PBuA_{0.46})_{37K}$ (BCP4).

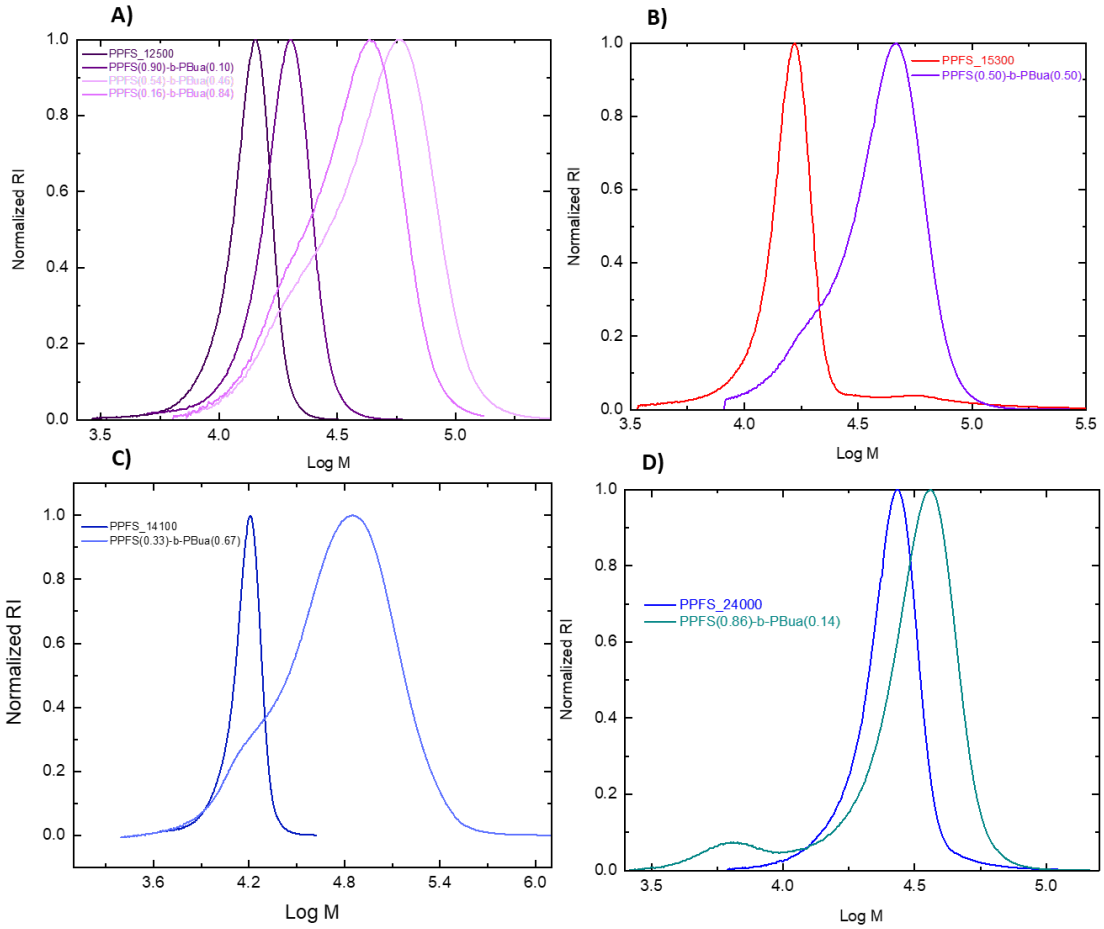

Figure SI 4. SEC chromatograms of (A) macro-initiator (PPFS1) (Mn = 12 500 g/mol, Mw = 13 400 g/mol, ~~*Đ*~~ = 1.07) and [$(PPFS_{0.90}$-*b*-$PBuA_{0.10})_{17K}$ BCP6 (Mn = 17 400 g/mol, D = 1.09); $(PPFS_{0.54}$-*b*-$PBuA_{0.46})_{37K}$ BCP4 (Mn = 37 000 g/mol, D = 1.36); $(PPFS_{0.16}$-*b*-$PBuA_{0.84})_{31K}$ BCP1 (Mn = 31 000 g/mol, D = 1.26)] - chain extension from PPFS1.

(B) macro-initiator (PPFS3) (Mn = 15 300 g/mol, Mw = 16 100 g/mol, ~~*Đ*~~ = 1.05) and ($PPFS_{0.50}$-*b*-$PBuA_{0.50})_{34K}$ BCP3 (Mn = 34 000 g/mol, D = 1.2) - chain extension from PPFS3.

(C) macro-initiator (PPFS2) (Mn = 14 100 g/mol, Mw = 15 200 g/mol, ~~*Đ*~~ = 1.07) and ($PPFS_{0.33}$-*b*-$PBuA_{0.67})_{40K}$ BCP2 (Mn = 40 100 g/mol, D = 1.88) - chain extension from PPFS2.

(D) macro-initiator (PPFS4) (Mn = 24 000 g/mol, Mw = 26 400 g/mol, ~~*Đ*~~ = 1.1) and ($PPFS_{0.86}$-*b*-$PBuA_{0.14})_{31K}$ BCP5 (Mn = 30 600 g/mol, D = 1.12) - chain extension from PPFS4.

- DSC of the block copolymers

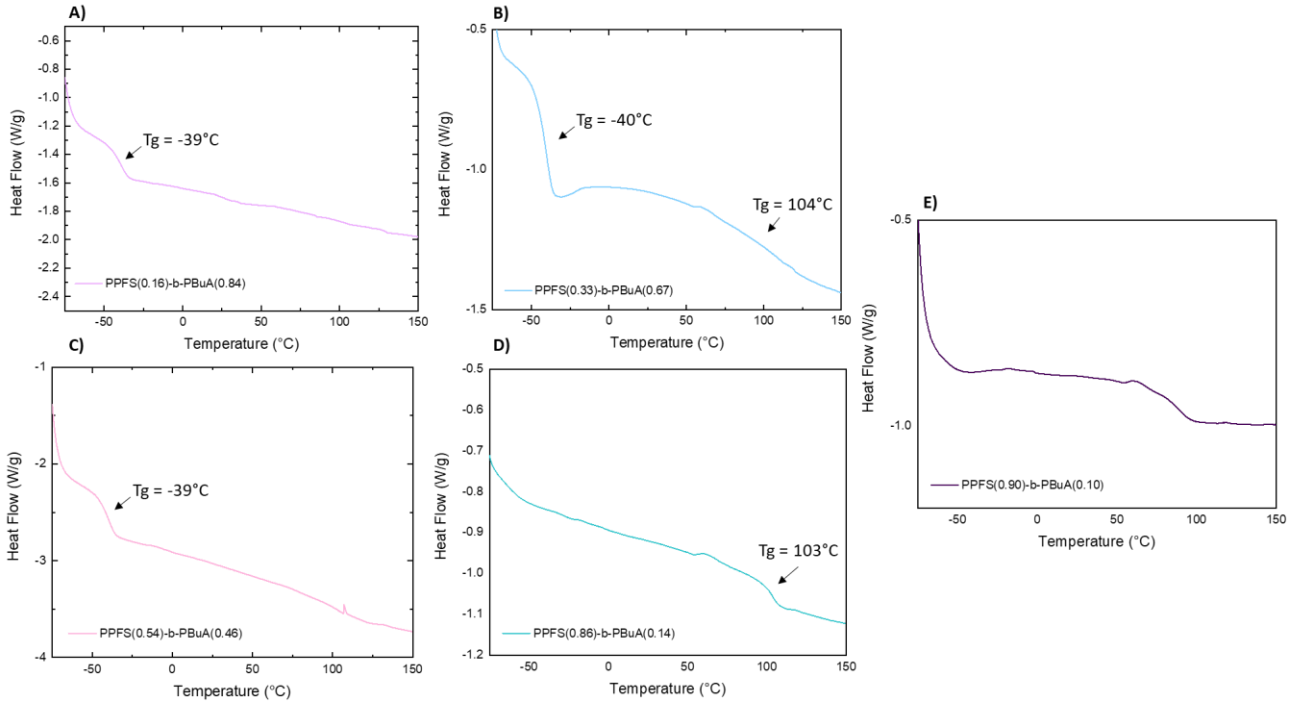

Figure SI 5. DSC of block copolymers ; (A) $(PPFS_{0.16}$-*b*-$PBuA_{0.84})_{31K}$ BCP1, (B) $(PPFS_{0.33}$-*b*-$PBuA_{0.67})_{40K}$ BCP2, (C) $(PPFS_{0.54}$-*b*-$PBuA_{0.46})_{37K}$ BCP4, (D) $(PPFS_{0.86}$-*b*-$PBuA_{0.14})_{31K}$ BCP5, (E) $(PPFS_{0.90}$-*b*-$PBuA_{0.10})_{17K}$ BCP6.

- DSC of 1-hexanethiol modified $PPFS_{0.33}$-*b*-$PBuA_{0.67}$ (BCP2)

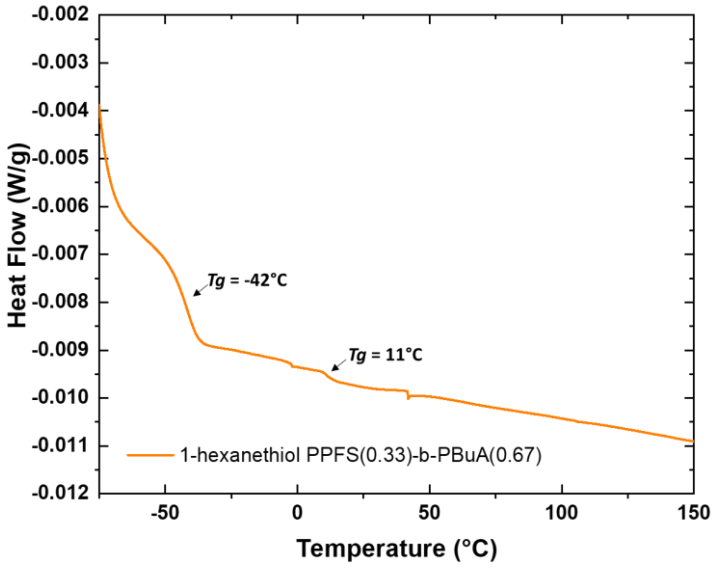

Figure SI 6. DSC of 1-hexanethiol modified $PPFS_{0.33}$-*b*-$PBuA_{0.67}$ BCP2.

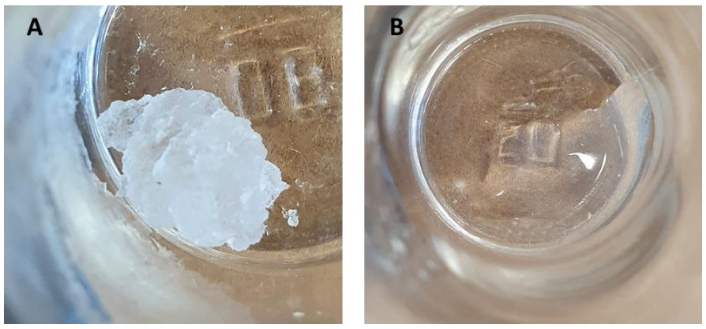

Figure SI 7. (A) BCP3 $(PPFS_{0.33}$-*b*-$PBuA_{0.67})_{40K}$ polymer at room temperature, (B) BCP3 modified with 1-hexanethiol at room temperature.

- SAXS peaks attribution:

The attribution of the peaks was made using the Primus software an following the distance distribution placement of the peaks. Indeed, some peaks that were not as intense on the original graph were visible using this functionality of the software.

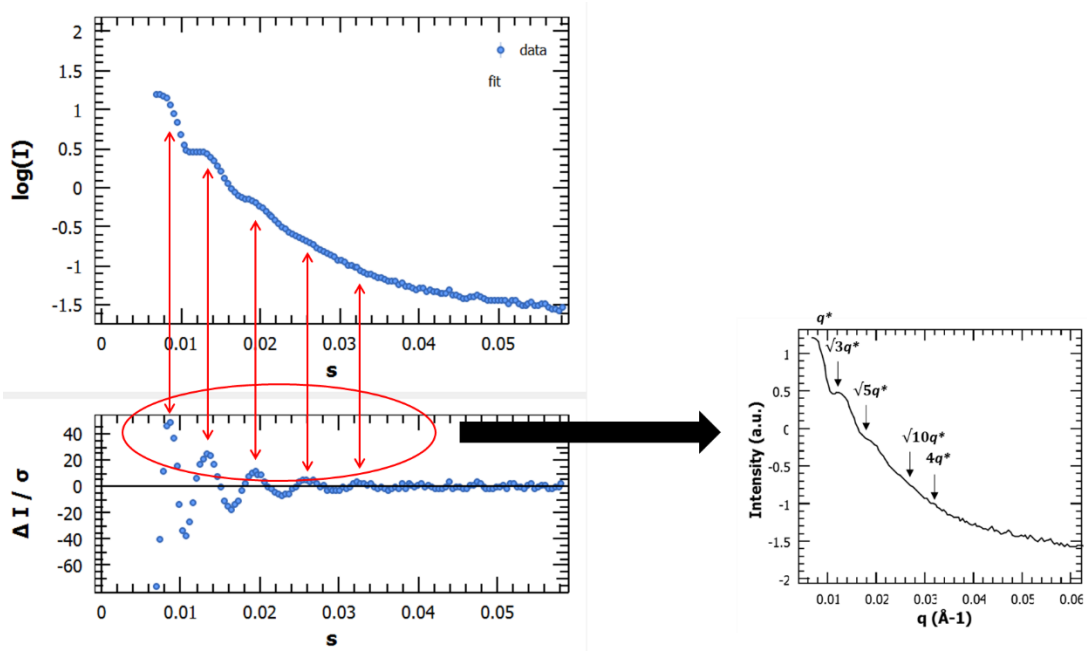

- Distance between nanodomains (SAXS):

Depending on the spacing between scattering vectors (q) and the structure of the material, the distance between nanodomains is calculated using different formulas. The choice of one over the other depends on the type of periodic structure and the number of dimensions involved. Indeed, for a one-dimensional periodic structure such as the lamellar (LAM) structure, equation (1) will be used; For a two-dimensional structure such as hexagonally closed-packed cylinders (HCC), equation (2) will be used and finally; equation (3) is for a three-dimensional structure such as primitive cubic or body centered cubic (BCC). The dimensions in the equations are represented by the Miller indices: h, k, l. (36)

Equation SI 4. Determination of the distance between nanodomains.

$q = (4\,\pi\,\sin\theta\,/\,\lambda)$

(1) $q_n = (n\,2\,\pi\,/\,d) \rightarrow d = (n\,2\,\pi\,/\,q)$

(2) $q_n = (4\,\pi\,/\,\sqrt{3}\,d)\,\sqrt{(h^2 + k^2 + hk)} \rightarrow d = (4\,\pi\,/\,\sqrt{3}\,q_n)\,\sqrt{(h^2 + k^2 + hk)}$

(3) $q_n = (2\,\pi\,/\,d)\,\sqrt{(h^2 + k^2 + l^2)} \rightarrow d = (2\,\pi\,/\,q_n)\,\sqrt{(h^2 + k^2 + l^2)}$

$$q = \frac{4\,\pi\,\sin\theta}{\lambda}$$

(1) $$q_n = n\,\frac{2\pi}{d} \longrightarrow d = \frac{2\pi n}{q}$$

(2) $$q_n = \frac{4\pi}{\sqrt{3}\,d}\sqrt{h^2 + k^2 + hk} \longrightarrow d = \frac{4\pi}{\sqrt{3}\,q_n}\sqrt{h^2 + k^2 + hk}$$

(3) $$q_n = \frac{2\pi}{d}\sqrt{h^2 + k^2 + l^2} \longrightarrow d = \frac{2\pi}{q_n}\sqrt{h^2 + k^2 + l^2}$$

Experimentally for each block copolymer the peaks positions are:

Table SI 1. SAXS peak position of the block copolymers and the block copolymer modified with 1-hexanethiol.

Block copolymer	q ($Å^{-1}$)	Peak position ratios	Pitch (nm)	Lattice structure
(PPFS$_{0.16}$-*b*-PBuA$_{0.84}$)$_{31K}$	0.0161 0.0288 0.0428 0.058	1 $\sqrt{3}$ $\sqrt{7}$ $\sqrt{13}$	45	HCC
(PPFS$_{0.33}$-*b*-PBuA$_{0.67}$)$_{40K}$	0.016 0.0271 0.0446 0.0582	1 $\sqrt{3}$ $\sqrt{7}$ $\sqrt{13}$	45	HCC
(PPFS$_{0.50}$-*b*-PBuA$_{0.50}$)$_{34K}$	0.018 0.0361 0.0541 0.0718	1 2 3 4	35	LAM
(PPFS$_{0.54}$-*b*-PBuA$_{0.46}$)$_{37K}$	0.0158 0.0329 0.055	1 2 $\sqrt{12}$	45	HCC
(PPFS$_{0.86}$-*b*-PBuA$_{0.14}$)$_{31K}$	0.0228 0.0409 0.048 0.0686	1 $\sqrt{3}$ 2 3	32	HCC
(PPFS$_{0.90}$-*b*-PBuA$_{0.10}$)$_{17K}$	0.039	1	-	disorder

$PPFS_{0.24}$-*b*-$PbuA_{0.76}$ (Tuned from ($PPFS_{0.16}$-*b*-$PBuA_{0.84}$)$_{31K}$)	0.0167	1	38	Cubic
	0.024	$\sqrt{2}$		
	0.0285	$\sqrt{3}$		
	0.0347	2		
	0.0403	$\sqrt{6}$		
$PPFS_{0.59}$-*b*-$PbuA_{0.41}$ (Tuned from ($PPFS_{0.54}$-*b*-$PBuA_{0.46}$)$_{37K}$)	0.0162	1	45	HCC
	0.0317	2		
	0.0473	3		
	0.0604	$\sqrt{13}$		
1-hexanethiol modified $PPFS_{0.33}$-*b*-$PBuA_{0.67}$	0.017	1	43	disorder